

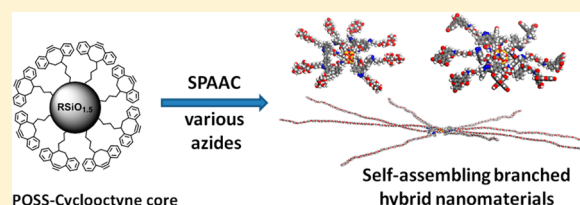
## Branched Polyhedral Oligomeric Silsesquioxane Nanoparticles Prepared via Strain-Promoted 1,3-Dipolar Cycloadditions

Petr A. Ledin,<sup>†</sup> Weinan Xu,<sup>†</sup> Frédéric Friscourt,<sup>‡</sup> Geert-Jan Boons,<sup>‡,§</sup> and Vladimir V. Tsukruk<sup>\*,†</sup><sup>†</sup>School of Materials Science and Engineering, Georgia Institute of Technology, Atlanta, Georgia 30332, United States<sup>‡</sup>Complex Carbohydrate Research Center and <sup>§</sup>Department of Chemistry, University of Georgia, Athens, Georgia 30602, United States

## S Supporting Information

**ABSTRACT:** Conjugation of small organic molecules and polymers to polyhedral oligosilsesquioxane (POSS) cores results in novel hybrid materials with unique physical characteristics. We report here an approach in which star-shaped organic–inorganic scaffolds bearing eight cyclooctyne moieties can be rapidly functionalized via strain-promoted azide–alkyne cycloaddition (SPAAC) to synthesize a series of nearly monodisperse branched core–shell nanoparticles with hydrophobic POSS cores and hydrophilic arms.

We established that SPAAC is a robust method for POSS core octafunctionalization with the reaction rate constant of  $1.9 \times 10^{-2} \text{ M}^{-1} \text{ s}^{-1}$ . Functionalization with poly(ethylene glycol) (PEG) azide, fluorescein azide, and unprotected lactose azide gave conjugates which represent different classes of compounds: polymer conjugates, fluorescent dots, and bioconjugates. These resulting hybrid compounds were preliminarily tested for their ability to self-assemble in solution and at the air–water interface. We observed the formation of robust smooth Langmuir monolayers with diverse morphologies. We found that polar lactose moieties are completely submerged into the subphase whereas the relatively hydrophobic fluorescein arms had extended conformation at the interface, and PEG arms were partially submerged. Finally, we observed the formation of stable micelles with sizes between 70 and 160 nm in aqueous solutions with size and morphology of the structures dependent on the molecular weight and the type of the peripheral hydrophilic moieties.



## ■ INTRODUCTION

Well-defined organic–inorganic cubic cage nanostructures of general formula  $\text{RSiO}_{3/2}$ , termed polyhedral oligosilsesquioxanes (POSS), have become attractive functional cores due to their thermal stability, monodispersity, ease of preparation, and covalent functionalization.<sup>1–3</sup> Conjugation of small organic molecules and polymers to POSS core results in novel hybrid materials with unique physical characteristics and improved thermal, mechanical, and optical properties.<sup>4</sup> For example, tethering of organic chromophores to POSS core was shown to increase their thermal and photostability, enhance their optical properties, and impart solution processability, allowing the manufacture of nanocomposites by common top-down fabrication methods.<sup>5–8</sup> Furthermore, the materials where the POSS core was modified with poly(ethylene glycol) (PEG) or ionic liquid (IL) moieties were utilized for energy storage and conversion.<sup>9–11</sup> The conjugation of biologically active molecules to the nontoxic and biocompatible POSS core is highly desirable for applications in drug delivery and bioimaging where multivalency is required.<sup>12</sup>

Starlike molecules with inorganic POSS core and organic arms of polymeric or monomeric nature are of particular interest, as they possess unique properties that are not observed in their linear counterparts.<sup>13</sup> Branched POSS-based materials have shown self-assembly properties in bulk, in solution, and at interfaces.<sup>14,15</sup> Depending on conditions such compounds can

exist as unimolecular vesicles or aggregate into polymer-somes.<sup>16,17</sup> Starlike architecture also defines the bulk properties of these materials, providing three-dimensional scaffolding for supramolecular assembly and cross-linking.<sup>18,19</sup> Finally, an increased free volume in thin films prepared from star-shaped POSS conjugates lowers the dielectric constant, allows for unhindered azobenzene photoisomerization, and improves antifouling properties.<sup>20–22</sup>

The traditional synthetic protocols, usually exploited for the chemical modification of POSS cores, such as hydrosilylation, often require harsh reaction conditions and prolonged reaction times and may lead to mixtures of polydisperse partially modified cores.<sup>23,24</sup> In contrast, “click” reactions such as thiol–ene/yne additions, formation of disulfide bonds, Diels–Alder reactions, and 1,3-dipolar cycloadditions can be highly efficient and tolerate a wide range of functional groups facilitating the practical construction of POSS-based hybrid nanoparticles.<sup>13,25</sup> Copper-catalyzed azide–alkyne cycloaddition (CuAAC), the most explored of these click reactions, can also be used for grafting polymers, dyes, peptides, and carbohydrates onto the POSS core.<sup>26–30</sup>

Received: May 13, 2015

Revised: June 29, 2015

Published: July 1, 2015

On the other hand, strain-promoted azide–alkyne cycloadditions (SPAAC) offer advantages similar to CuAAC but do not require either the use of toxic copper catalyst or extensive optimization of reaction conditions.<sup>31,32</sup> Moreover, the stable cyclic alkynes, such as 4-dibenzocyclooctynol (DIBO), are easy to prepare and react rapidly with 1,3-dipoles (azides, nitrones, nitrile oxides, and diazo compounds) and 1,2,4,5-tetrazines.<sup>33–36</sup> Because SPAAC requires no catalyst, generates a stable triazole moiety, and gives no byproducts, it is increasingly employed during construction and functionalization of hydrogels, polymers, and dendrimers.<sup>37–40</sup> Recently, Su and Li et. al demonstrated the versatility of SPAAC by sequential multifunctionalization of POSS scaffolds where SPAAC has been used in tandem with other orthogonal click reactions to produce linear and cyclic polymeric surfactants with hydrophilic POSS head groups.<sup>41–44</sup> However, to the best of our knowledge, no starlike compounds have been synthesized using this efficient synthetic approach with potentially practical multifunctional hybrid nanomaterials.

We therefore contemplated that a cubic octavalent oligosilsesquioxane bearing strained alkynes as corner functionalities could serve as a functional scaffold for the facile construction of starlike or branched core–shell nanoparticles via the SPAAC approach with minimal incomplete derivatization and product inhomogeneity. In this study, we demonstrated that this approach can be efficiently applied to coupling azide-containing fluorescent dyes and hydrophilic moieties such as carboxyfluorescein, lactose, and PEGs to give a library of nearly monodisperse branched organic–inorganic hybrid nanoparticles a few nanometers in diameter under mild reaction conditions. The conjugation of hydrophilic moieties to the POSS-based scaffold resulted in diverse self-assembly behavior at the air–water interface as well as in aqueous solutions driven by the hydrophobic POSS core with the morphology of the structures dependent on the molecular weight and the type of the peripheral hydrophilic moieties.

## EXPERIMENTAL SECTION

**Materials.** Octaammonium POSS hydrochloride was purchased from Hybrid Plastics. *N,N*-Diisopropylethylamine (99.5%) was purchased from Sigma-Aldrich. Dichloromethane (DCM) was distilled over calcium hydride prior to use. The azido-modified fluorescein **4** was prepared as described previously.<sup>45</sup> The 2-azidopentyl  $\beta$ -D-galactopyranosyl-(1 $\rightarrow$ 4)- $\beta$ -D-glucopyranoside (**5**) and azido-PEG derivatives **6** and **7** were prepared as described previously.<sup>39</sup> Reactions were performed at room temperature (20–22 °C), unless stated otherwise.

**NMR.** The NMR spectra were recorded on Varian Mercury (300, 500 MHz) and Bruker DMX 400 (400 MHz) spectrometers at 25 °C. Chemical shifts are reported in  $\delta$  units, parts per million (ppm) downfield from TMS; spectra are referenced by solvent signals. Only proton spectra are provided for SPAAC conjugates due to complexity of carbon spectra because of 1,2,3-triazole regioisomeric mixture.

**Molecular Weight.** Mass spectra were obtained using MALDI-TOF instruments (ABISciex 5800 MALDI-TOF-TOF) with 2,5-dihydroxybenzoic acid as a matrix in positive reflector mode unless stated otherwise. The Shimadzu LCMS-IT-TOF was used to obtain and ESI-MS spectrum in negative mode. Monoisotopic masses are provided unless stated otherwise. Gel permeation chromatography (GPC) analysis was performed on a Shimadzu instrument equipped with a LC-20AD HPLC pump and a refractive index detector (RID-10A, 120 V). THF was used as the mobile phase at the flow rate of 1.0 mL/min at 35 °C. One Phenogel 5  $\mu$ m linear column and one Phenogel 5  $\mu$ m 10E4A mixed bead column were used in series. Molecular weights were calculated against polystyrene standards.

**TEM.** The TEM was done using a JEOL 100CX operated at 100 kV with samples drop-cast on carbon–Formvar-coated copper grids (Ted Pella, Inc.). The excess of water was removed by touching the edge of the grids with a small piece of filter paper (Whatman). The grids were allowed to dry at room temperature followed by staining with a drop of 2 wt % phosphotungstic acid (freshly prepared in Nano pure water and filtered through a 0.2  $\mu$ m filter membrane). After 2 min, excess staining agent was removed by blotting with filter paper, and the grids were further dried at ambient temperature for 15 min and used for TEM imaging.

**DLS.** Dynamic light scattering measurements were performed using a laser light scattering spectrometer (Malvern Zetasizer Nano ZS) at 25 °C. For each sample, 12–14 replicates were obtained to determine the average and mean sizes and size distribution. The polydispersity of sizes of polymeric self-assembled structures (polydispersity index) is equal to  $(\sigma/d)^2$ , where  $\sigma$  is a standard deviation and  $d$  is the mean diameter of the particles. Critical micellar concentration was determined by observing a count rate for samples with different concentrations of **8–11** in water prepared by serial dilution.

**Langmuir–Blodgett Deposition.** A KSV2000 LB minitrough filled with Nanopure water (18.2 M $\Omega$  cm) at room temperature was used for LB deposition. The surface pressure was measured with a platinum Wilhelmy plate attached to a pressure sensor. The solution of compounds (0.1 mg/mL in 10% MeOH in CHCl<sub>3</sub> (vol) or EtOH:CHCl<sub>3</sub>, 9:1 (v:v), for compound **8**) was carefully spread over the water surface, and the monolayer was left for 30 min to allow for evaporation of the organic solvent and equilibration. The Langmuir monolayer was then compressed at a rate of 5 mm/min to reach a surface pressure of 1, 4, or 6 mN/m. The monolayer was transferred onto precleaned silicon slide at the air–water interface by pulling the substrate up vertically at a rate of 1 mm/min. Silicon wafers were cleaned with piranha solution (3:1 concentrated sulfuric acid and hydrogen peroxide mixture; *caution*: strong oxidizer!) according to the known procedure.<sup>46</sup> Then wafers were rinsed thoroughly with nanopure water and dried with a nitrogen stream. The value of the limiting cross-sectional area in condensed state,  $A_0$ , was derived from pressure–area isotherms by using the tangent line corresponding to the steepest rise in the surface pressure.

**AFM.** AFM images were obtained using a Dimension-3000 (Digital Instruments) microscope in the “light” tapping mode according to the well-established procedure.<sup>47</sup> Image processing was performed using NanoScope 1.40 and Gwyddion 2.36 software.

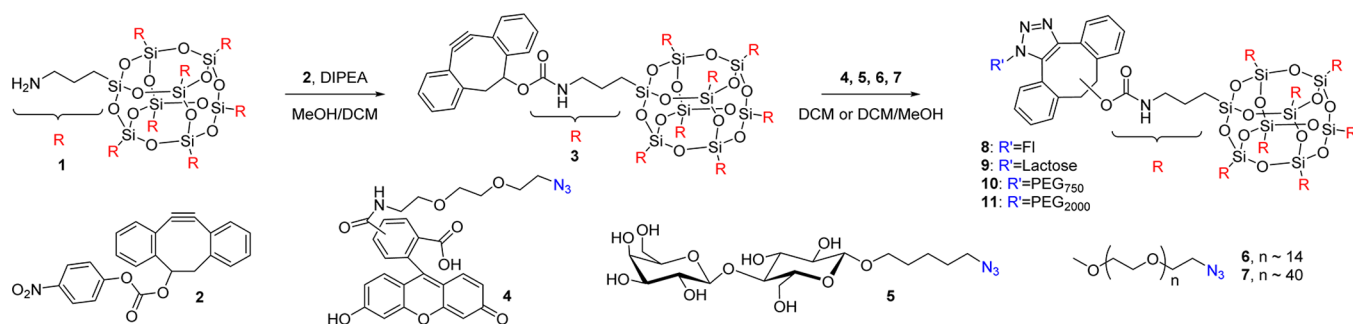
**Spectrophotometry.** The UV–vis spectra were recorded on Shimadzu UV-2450 spectrophotometer in 1 cm quartz spectrophotometric cells. Fluorescence spectra were acquired on Shimadzu RF-5301pc spectrofluorophotometer. FTIR spectra were obtained on Bruker Vertex 70 spectrometer in KBr pellets.

**Molecular Modeling.** Molecular models were built with Accelrys Materials Studio 3.1. The structures were optimized using the Discover tool (CVFF force field). The minimal cross section (molecular area) was calculated from the smallest sectional diameter of the molecules with hydrophilic arms “submerged” into the subphase.

**Spectroscopic Ellipsometry.** Spectroscopic ellipsometry was performed with a M-2000U ellipsometer (Woollam). The spectral range was 245–1000 nm (D2 and QTH lamps). Ellipsometry data from all samples were acquired at 65°, 70°, and 75° angles of incidence over the spectral range. The monolayers were fitted with a three-layer model which consists of a silicon substrate, a silicon oxide layer (2 nm layer thickness), and a Cauchy layer (MSE < 1.5) in the range from 400 to 1000 nm. The average values of three measurements with standard deviation are provided.

**Synthesis.** Synthesis of POSS(DIBO)<sub>8</sub> (**3**). Octaammonium POSS hydrochloride was desalted using a procedure reported by Feher et al. to give **1**.<sup>48</sup> Specifically, the suspension of hydrochloride salt (90 mg, 0.078 mmol) in MeOH (50 mL) was passed through an Amberlite IRA-400 basic resin (washed repeatedly with 1 M NaOH and H<sub>2</sub>O prior to use). The resulting solution was then concentrated under reduced pressure to 10 mL and added to a stirred solution of carbonic acid 5,6-dihydro-11,12-didehydridibenzo[*a,e*]cycloocten-5-yl ester (**2**)<sup>49</sup> (300 mg, 0.78 mmol) and *N,N*-diisopropylethylamine (0.2

**Scheme 1. Synthesis of Functionalized Compound 3 from Octaamine POSS Core (1) and Its Subsequent Modification Using Fluorescein (4), Lactose (5), and PEG Azides (6, 7)<sup>a</sup>**



<sup>a</sup>Note that both 1,4- and 1,5-regioisomers of 1,2,3-triazoles 8–11 are formed in the SPAAC reaction.

mL, 1.17 mmol) in DCM (3 mL). After stirring overnight (10 h) at room temperature, the reaction mixture was concentrated under reduced pressure, and the residue was purified by column chromatography on silica gel using a gradient of 0–3% MeOH in DCM. Additional purification from *p*-nitrophenol was performed by size exclusion chromatography on Sephadex LH-20 gel using 50% MeOH in DCM as an eluent to give pure 3 as an off-white amorphous solid (166 mg, 74%). <sup>1</sup>H NMR (400 MHz, DMSO-*d*<sub>6</sub>)  $\delta$ : 0.25–0.58 (m, 16H, SiCH<sub>2</sub>), 1.10–1.70 (m, 16H, SiCH<sub>2</sub>CH<sub>2</sub>), 2.71 (app d, 8H, *J* = 11.9 Hz, CHCHH), 2.81–3.04 (m, 16H, NHCH<sub>2</sub>), 3.11 (d, 8H, *J* = 14.1 Hz, CHCHH), 5.28 (s, 8H, CHCH<sub>2</sub>), 7.01–7.92 (m, 64H, 8  $\times$  CH<sub>ar</sub>). <sup>13</sup>C NMR (100 MHz, DMSO-*d*<sub>6</sub>)  $\delta$ : 8.52 (SiCH<sub>2</sub>), 22.72 (SiCH<sub>2</sub>CH<sub>2</sub>), 42.61 (CHCH<sub>2</sub>), 45.50 (NHCH<sub>2</sub>), 75.30 (CHCH<sub>2</sub>), 109.90 (C $\equiv$ C), 112.59 (C $\equiv$ C), 120.38 (C<sub>ar</sub>), 122.90 (CH<sub>ar</sub>), 123.75 (C<sub>ar</sub>), 125.76 (CH<sub>ar</sub>), 126.09 (CH<sub>ar</sub>), 127.26 (CH<sub>ar</sub>), 127.31 (CH<sub>ar</sub>), 128.19 (CH<sub>ar</sub>), 128.30 (CH<sub>ar</sub>), 130.04 (CH<sub>ar</sub>), 150.84 (C=O), 152.47 (C<sub>ar</sub>), 155.25 (C<sub>ar</sub>). <sup>29</sup>Si NMR (80 MHz, DMSO-*d*<sub>6</sub>)  $\delta$ : -66.21 (s, O<sub>3</sub>SiCH<sub>2</sub>). FTIR (KBr, cm<sup>-1</sup>): 3500–3250 (s, NH), 3115–3000 (m, CH, arom), 2995–2816 (m, CH aliph), 1713 (s, C=O), 1515 (s, C=C, arom), 1476–1408 (m), 1244 (s, C–O), 1198 (m), 1119 (s, Si–O), 1037 (m), 756 (s). HRMS (MALDI) *m/z*: 2872.07 (C<sub>160</sub>H<sub>144</sub>NaN<sub>8</sub>O<sub>28</sub>Si<sub>8</sub> (MNa<sup>+</sup>), requires 2871.81); GPC *M<sub>n</sub>* = 2100 g/mol, *D<sub>M</sub>* = 1.18.

General procedure for SPAAC reaction with 3. A solution of 3 (1 equiv) and corresponding azide (10 equiv) in a MeOH/DCM mixture (3 mL, 50% (vol)) (4, 5) or DCM (3 mL) (6, 7) was stirred for 18 h at room temperature. The solvent was removed under reduced pressure, and the residue was purified to give the title conjugates.

POSS(FI)<sub>8</sub> (8) (33 mg, 46% orange solid) was prepared from compounds 3 (30 mg, 0.01 mmol) and 4 (53 mg, 0.1 mmol). Purified by precipitating from cold hexanes (75 mL) twice. <sup>1</sup>H NMR (500 MHz, DMSO-*d*<sub>6</sub>)  $\delta$ : 0.29–0.64 (m, 16H, SiCH<sub>2</sub>), 1.32–1.67 (m, 16H, SiCH<sub>2</sub>CH<sub>2</sub>), 2.73–3.57 (m, 96H, CHCH<sub>2</sub>, NHCH<sub>2</sub>, CH<sub>2</sub>O), 3.72–3.90 (m, 16H, CH<sub>2</sub>O), 4.21–4.62 (m, 16H, NCH<sub>2</sub>), 5.67–6.20 (m, 8H, CH<sub>2</sub>CH), 6.44–6.76 (m, 48H, CH<sub>ar</sub>), 6.92–7.61 (m, 76H, NHCO, CH<sub>ar</sub>, CH<sub>ar</sub>-isomers), 7.69 (s, 4H, CH<sub>ar</sub>-isomers), 7.95–8.26 (m, 12H, CH<sub>ar</sub>-isomers), 8.45 (s, 4H, CH<sub>ar</sub>-isomers), 8.69 (s, 4H, NHCO-isomers), 8.83 (s, 4H, NHCO-isomers), 10.13 (s, 16H, OH). FTIR (KBr, cm<sup>-1</sup>): 3400 (br, s, NH, OH), 3073 (m, CH, arom), 2995–2799 (m, CH aliph), 1760 (s, C=O), 1696 (s, C=O), 1609 (s, C=C), 1506 (s, C=C, arom), 1454 (m), 1244 (s, C–O), 1173 (m), 1116 (s, Si–O), 997 (m), 858 (m), 768 (m). MS (MALDI, linear mode, molecular weight) *m/z*: 7164.21 (C<sub>376</sub>H<sub>336</sub>NaN<sub>40</sub>O<sub>92</sub>Si<sub>8</sub> (MNa<sup>+</sup>), requires 7134.68) fragmentation presumably with carbamate bond cleavage and loss of a 780 Da arms was observed (ESI, negative mode, molecular weight) *m/z*: 1776.58 (C<sub>376</sub>H<sub>332</sub>N<sub>40</sub>O<sub>92</sub>Si<sub>8</sub> (M-4H<sup>+</sup>), requires 1776.91).

POSS(Lac)<sub>8</sub> (9) (41 mg, 90%, white powder) was prepared from compounds 3 (20 mg, 0.007 mmol) and 5 (32 mg, 0.070 mmol). Purified by dialysis against water using a 3 kDa MWCO membrane. <sup>1</sup>H NMR (400 MHz, DMSO-*d*<sub>6</sub>)  $\delta$ : 0.31–0.74 (m, 16H, SiCH<sub>2</sub>), 1.07–1.60 (m, 48H, OCH<sub>2</sub>CH<sub>2</sub>CH<sub>2</sub>, SiCH<sub>2</sub>CH<sub>2</sub>), 1.64–1.83 (m, 16H,

NCH<sub>2</sub>CH<sub>2</sub>), 2.72–3.40 (m, 56H, CHCH<sub>2</sub>, OCH<sub>2</sub>, OCH, NHCH<sub>2</sub>), 3.45–3.79 (m, 88H, OHCH<sub>2</sub>CH, OHCH), 4.09–4.24 (m, 16H, CHO), 4.25–4.45 (m, 16H, NCH<sub>2</sub>), 4.49–4.61 (m, 16H, OH), 4.62–4.71 (m, 16H, OH), 4.75–4.87 (m, 8H, OH), 5.04–5.20 (m, 16H, OH), 5.72–6.23 (m, 8H, CHCH<sub>2</sub>), 6.84–7.67 (m, 72H, NHCO, CH<sub>ar</sub>). FTIR (KBr, cm<sup>-1</sup>): 3411 (br, s, NH, OH), 3064 (m, CH, arom), 2990–2800 (m, CH aliph), 1711 (s, C=O), 1512 (s, C=C, arom), 1483–1337 (m), 1251 (s, C–O), 1170–947 (s, C–O, Si–O), 894 (m), 768 (m). HRMS (MALDI, molecular weight) *m/z*: 6501.64 (C<sub>296</sub>H<sub>392</sub>NaN<sub>32</sub>O<sub>116</sub>Si<sub>8</sub> (MNa<sup>+</sup>), requires 6502.17).

POSS(PEG<sub>750</sub>)<sub>8</sub> (10) (140 mg, 88%, colorless oil) was prepared from compounds 3 (50 mg, 0.018 mmol) and 6 (135 mg, 0.18 mmol). Purified by size exclusion chromatography on Sephadex LH-20 gel using 50% MeOH in DCM as an eluent. <sup>1</sup>H NMR (500 MHz, CDCl<sub>3</sub>)  $\delta$ : 0.21–0.65 (m, 16H, SiCH<sub>2</sub>), 1.23–1.64 (m, 16H, SiCH<sub>2</sub>CH<sub>2</sub>), 2.71–3.23 (m, 32H, CHCH<sub>2</sub>, NHCH<sub>2</sub>), 3.31 (s, 24H, CH<sub>3</sub>O), 3.36–3.65 (m, 272H, CH<sub>2</sub>O), 3.67–4.12 (m, 32H, CH<sub>2</sub>O), 4.17–4.61 (m, 16H, NCH<sub>2</sub>), 4.99–5.46 (m, 8H, NH), 5.62–6.30 (m, 8H, CH<sub>2</sub>CH), 6.81–7.72 (m, 64H, CH<sub>ar</sub>). FTIR (KBr, cm<sup>-1</sup>): 3523 (br, s, NH), 3059 (m, CH, arom), 2871 (br, s, CH aliph), 1717 (s, C=O), 1640 (m), 1532 (s, C=C, arom), 1458 (s, CH), 1353 (s), 1280 (s, C–O), 1246 (s, C–O), 1170–1020 (s, C–O, Si–O), 955 (m), 850 (m), 766 (m). GPC *M<sub>n</sub>* = 6100 g/mol, *D<sub>M</sub>* = 1.11.

POSS(PEG<sub>2000</sub>)<sub>8</sub> (11) (320 mg, 91%, white powder) was prepared from compounds 3 (50 mg, 0.018 mmol) and 7 (360 mg, 0.18 mmol). Purified by dialysis against water using a 10 kDa MWCO membrane. <sup>1</sup>H NMR (400 MHz, CDCl<sub>3</sub>)  $\delta$ : 0.20–0.66 (m, 16H, SiCH<sub>2</sub>), 1.34–1.67 (m, 16H, SiCH<sub>2</sub>CH<sub>2</sub>), 2.73–3.27 (m, 32H, CHCH<sub>2</sub>, NHCH<sub>2</sub>), 3.35 (s, 24H, CH<sub>3</sub>O), 3.42–3.72 (m, 1392H, CH<sub>2</sub>O), 3.75–4.10 (m, 32H, CH<sub>2</sub>O), 4.23–4.68 (m, 16H, NCH<sub>2</sub>), 5.07–5.50 (m, 8H, NH), 5.70–6.35 (m, 8H, CH<sub>2</sub>CH), 6.97–7.88 (m, 64H, CH<sub>ar</sub>). FTIR (KBr, cm<sup>-1</sup>): 3450 (br, s, NH), 3056 (m, CH, arom), 2886 (br, s, CH aliph), 1718 (s, C=O), 1640 (m), 1535 (m, C=C, arom), 1467 (s, CH), 1342 (s), 1280 (s, C–O), 1240 (s, C–O), 1150–1057 (s, C–O, Si–O), 964 (s), 843 (s). GPC *M<sub>n</sub>* = 14 150 g/mol, *D<sub>M</sub>* = 1.06.

## RESULTS AND DISCUSSION

**Preparation and Characterization of Branched POSS Amphiphiles.** A cubic octavalent oligosilsesquioxanes bearing strained alkynes could serve as a functional scaffold for the facile construction of starlike or branched core–shell nanoparticles via SPAAC with minimal incomplete derivatization and product inhomogeneity. We started with the synthesis of a novel reactive POSS derivative 3 modified by eight dibenzocyclooctynol moieties (Scheme 1).

Thus, commercially available octaammonium POSS hydrochloride was first desalted to generate the free amines by passing it through a basic resin, yielding compound 1. Then, the octaamine 1 was reacted in the presence of Hünig's base



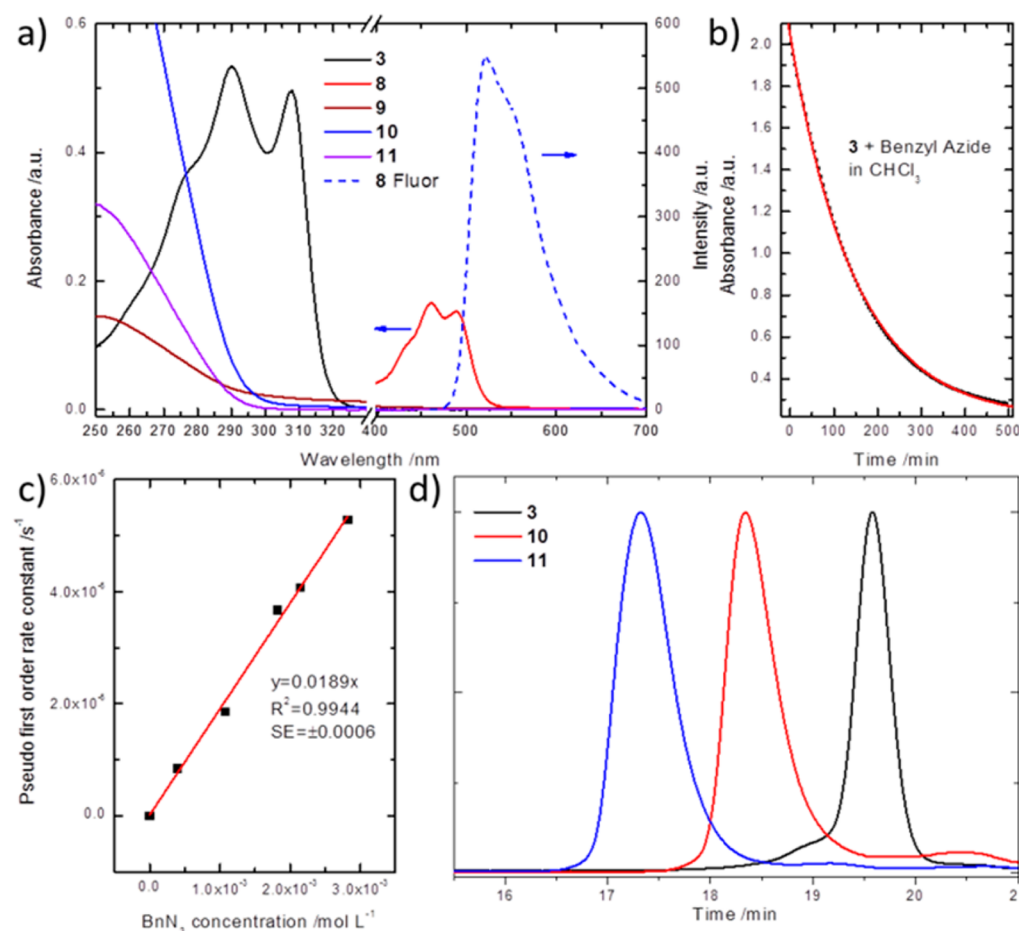


**Figure 1.** Characterization of POSS conjugates. (a) UV-vis spectra of **3** in  $\text{CHCl}_3$  (0.01 mg/mL) and conjugates **8**, **9** (0.01 mg/mL, 10% MeOH in  $\text{CHCl}_3$  (vol)) and **10**, **11** in  $\text{CHCl}_3$  (0.1 mg/mL) and emission spectrum of **8**. (b) Exponential decay of the absorbance of compound **3** ( $2.3 \times 10^{-5}$  M) at 306 nm wavelength treated with benzyl azide ( $2.5 \times 10^{-3}$  M) in  $\text{CHCl}_3$ . (c) Analysis of a second-order rate constant. (d) GPC traces of compounds **3**, **10**, and **11**.

**Table 1.** Characteristics of Compounds **3**–**11** and Their Micellar Self-Assemblies

compd	GPC data			DLS data		
	$M_n$ , g/mol (calc)	$M_n$ , g/mol	$\bar{D}_M^c$	Z-average diameter, nm	average diameter, nm	polydispersity index
<b>3</b>	2848	2100	1.18			
<b>8</b>	7111			69.5	43.2	0.12
<b>9</b>	6479			76.0	25.8	0.43
<b>10</b>	9650 <sup>a</sup>	6100	1.11	162.1	103.2	0.21
<b>11</b>	19550 <sup>b</sup>	14150	1.06	106.9	56.8	0.19

<sup>a</sup>Based on a number-average DP of PEG = 14. <sup>b</sup>Based on a number-average DP of PEG = 40. <sup>c</sup>Molar-mass dispersity ( $\bar{D}_M = M_w/M_n$ ).

with a slight excess of DIBO-carbonate (**2**) (1.2 equiv per group) that was prepared as previously described.<sup>49,50</sup>

The formation of the carbamate bond was monitored using mass spectrometry (MS) and thin layer chromatography and was found to be complete after 10 h. It has to be noted that octaamine **1** is rather unstable and prone to hydrolysis hence the use of a freshly desalted amine and excess of electrophile are needed.<sup>48</sup> The cyclooctyne-modified POSS **3** was isolated by column chromatography on silica gel and subsequently by size exclusion chromatography (SEC) on Sephadex LH-20 gel in 74%. The successful installation of eight cyclooctyne moieties was confirmed by MS, nuclear magnetic resonance spectrometry (NMR), and gel permeation chromatography (GPC) (see Supporting Information for spectra).

The strained carbon–carbon triple bond of cyclooctynes reacts rapidly with 1,3-dipoles such as azides, nitrones, and nitrile oxides to yield stable triazoles, isoxazolines, and isoxazoles, respectively. With a reactive scaffold for SPAAC in hand, we first evaluated the rate of 1,3-dipolar cycloaddition between **3** and benzyl azide by monitoring the decay of characteristic absorbance of DIBO at 306 nm in chloroform solution at 25 °C (Figure 1a,b). We used an excess of benzyl azide to obtain pseudo-first-order rate constants for different concentrations of benzyl azide. Subsequently a second-order rate constant of  $(1.89 \pm 0.06) \times 10^{-2} \text{ M}^{-1} \text{ s}^{-1}$  was obtained (Figure 1c) from the slope of a plot of pseudo-first-order rate constants vs benzyl azide concentration. This value is significantly lower than determined previously for the SPAAC of an unmodified DIBO molecule ( $0.058 \text{ M}^{-1} \text{ s}^{-1}$ ), which can

be explained by the steric bulk of eight cyclooctyne moieties confined to a 1 nm sized POSS core.<sup>39</sup> Nevertheless, octamodification of **3** by SPAAC with carboxyfluorescein azide (**4**), hydrophilic 2-azidopentyl  $\beta$ -D-galactopyranosyl-(1 $\rightarrow$ 4)- $\beta$ -D-glucopyranoside (lactose azide, **5**), and PEG azides (**6**, **7**) with different molecular weights (750 and 2000 g/mol, respectively) did proceed to completion (Scheme 1). Thus, core **3** was treated with 1.2 equiv of the respective azide for each DIBO moiety in DCM for PEG derivatives **6** and **7** and DCM:MeOH (3:1, v:v) for fluorescein azide **4** and lactose azide **5**. The corresponding conjugates were purified by precipitation with hexanes (**8**), size exclusion chromatography (**10**; Sephadex LH-20, 50% MeOH in DCM (vol)), or dialysis against water (**9**, **11**; 3 and 10 kDa molecular weight cutoff (MWCO), respectively). The SPAAC reaction was monitored by UV-vis spectrophotometry, following the disappearance of carbon-carbon triple bond absorption at around 306 nm (Figure 1b).

Physical properties of hybrid conjugates are summarized in Figure 1 and in Table 1. The fluorescein-modified POSS **8** displayed a strong fluorescence with absorption and emission profiles essentially identical to that of individual azido-modified fluorescein **4**. However, the quantum yield of the POSS-fluorescein conjugate is reduced significantly as compared to the unmodified dye **4** (Figure S1) possibly due to the confinement created by tethering the fluorophore to the small POSS core (**8** is 3–6.2 nm in diameter according to molecular modeling).<sup>27</sup> Close proximity of the fluorescein moieties can result in the energy transfer between dye molecules, leading to quenching.<sup>51,52</sup>

GPC analysis of the POSS-PEG conjugates **10** and **11** showed the expected increase in molecular weight from “apparent” 2100 g/mol (2850 g/mol theoretical) (**3**) to 6100 g/mol (9650 g/mol theoretical) (**10**) and 14 150 g/mol (19 550 g/mol theoretical) (**11**) (Table 1). A lower “apparent” molecular weight values obtained for all the POSS conjugates is common for branched molecules measured in comparison to the polystyrene GPC standards.<sup>53</sup> On the other hand, the GPC measurements show that the molar mass dispersity ( $\bar{D}_M$ ) of all the POSS conjugates synthesized here is very low (Figure 1d). The  $\bar{D}_M$  below 1.2 indicates the uniform functionalization of the POSS core.

The molecular weight of compounds **3** and **8–10** was confirmed by mass spectrometry (Supporting Information). We noted the decrease in signal intensity after SPAAC conjugation that can be explained by the partial loss of organic arms due to the cleavage of carbamate bond during the ionization process. For instance, a loss of a 700 Da lactose fragment was observed for compound **9**. Next, NMR spectroscopy was used to determine the degree of functionalization of POSS-conjugates **8–11**. The integral area of the peak corresponding to POSS  $\text{CH}_2$ -Si groups at 0.5 ppm was compared to a representative peak of  $\text{CH}_2\text{N}$ -triazole group at ca. 4.5 ppm (see NMR spectra in Supporting Information). Accordingly, the degree of functionalization of compounds **8**, **9**, **10**, and **11** was determined to be very high: 95%, 90%, 96%, and quantitative, respectively. The successful grafting of azides onto POSS core was additionally confirmed by IR spectroscopy, which showed the absence of azide stretching band at  $2110\text{ cm}^{-1}$  and the presence of both sets of signals from POSS core (Si-C at  $1250\text{ cm}^{-1}$ , Si-O-Si at  $1100\text{ cm}^{-1}$ ) and grafted arms (C-H  $2890\text{ cm}^{-1}$  (**10**, **11**); C-O  $1110\text{ cm}^{-1}$  (**9**, **10**, **11**); amide C=O  $1760\text{ cm}^{-1}$  (**8**)) (Figures S2 and S3).

**Assembly at the Air–Water Interface.** Next, we examined the possibility that monodisperse branched POSS conjugates **8–11**, which contain hydrophilic arms and hydrophobic core, can self-assemble in aqueous environment and at the air–water interface.<sup>17</sup> When solutions of amphiphilic compounds **8** (EtOH: $\text{CHCl}_3$ , 9:1, (v:v)) and **9–11** (0.1 mg/mL, 10% MeOH in  $\text{CHCl}_3$  (vol)) were spread at the air–water interface followed by the gradual compression of the Langmuir monolayer, we observed stable pressure–area isotherms (Figure 2).

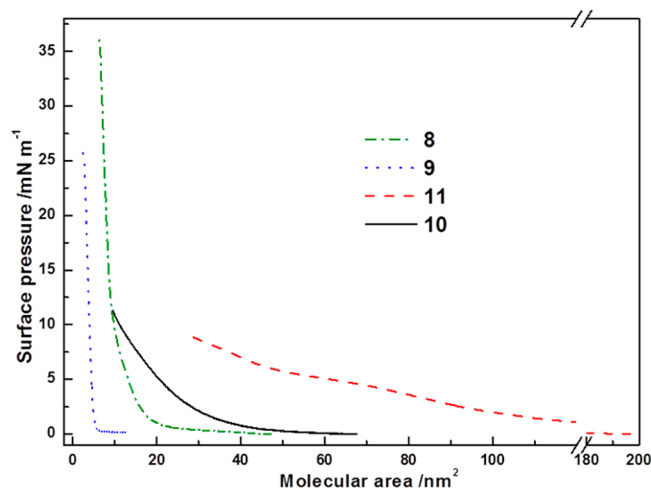


**Figure 2.** Pressure–area isotherms of POSS conjugates at the air–water interface.

This behavior indicates the formation of robust Langmuir monolayers similarly to that observed for partially hydrophobized POSS compounds with amphiphilic nature of side groups.<sup>54</sup> The conformation of amphiphilic molecules at the air–water interface can be evaluated by comparing the dimensions of the molecules based on computer simulations with experimental molecular areas obtained by the Langmuir technique or other methods.<sup>55</sup> By using molecular modeling (Materials Studio 3.1), we estimated the cross-sectional area of compounds **8–11** with different side chain conformations. We considered two scenarios: the hydrophilic arms are completely submerged into the subphase (minimum area) or extended parallel to the interphase (maximum area) (Figure 3 and Table 2). The structures of **8–11** with submerged arms are rotated  $-90^\circ$  relative to the interface in Figures 3b–e. Furthermore, the molecular model of **3** is added for comparison (Figure 3a). Because of the relatively short organic arms, bearing DIBO moieties, the optimized structure of **3** is almost spherical with a cross section of  $4.3\text{ nm}^2$ . However, after SPAAC functionalization the hydrophilic arms with relatively long spacers have enough rotational freedom to form segregated structures with hydrophobic POSS core on one end and a hydrophilic moiety (fluorescein, lactose, or PEG) on the other end. The limiting molecular area for amphiphiles **8–11** with submerged arms is chiefly determined by the molecular area of the hydrophobic POSS core of compound **3**, which is close to  $4\text{--}5\text{ nm}^2$ , in line with our previous observations.<sup>54</sup>

On the other hand, the maximum cross section reflects the molecular weight of grafted hydrophilic arms and is approximately  $25\text{--}30\text{ nm}^2$  for compounds **8** and **9** and  $139$  and  $790\text{ nm}^2$  for compounds **10** and **11**, respectively (Figure 3

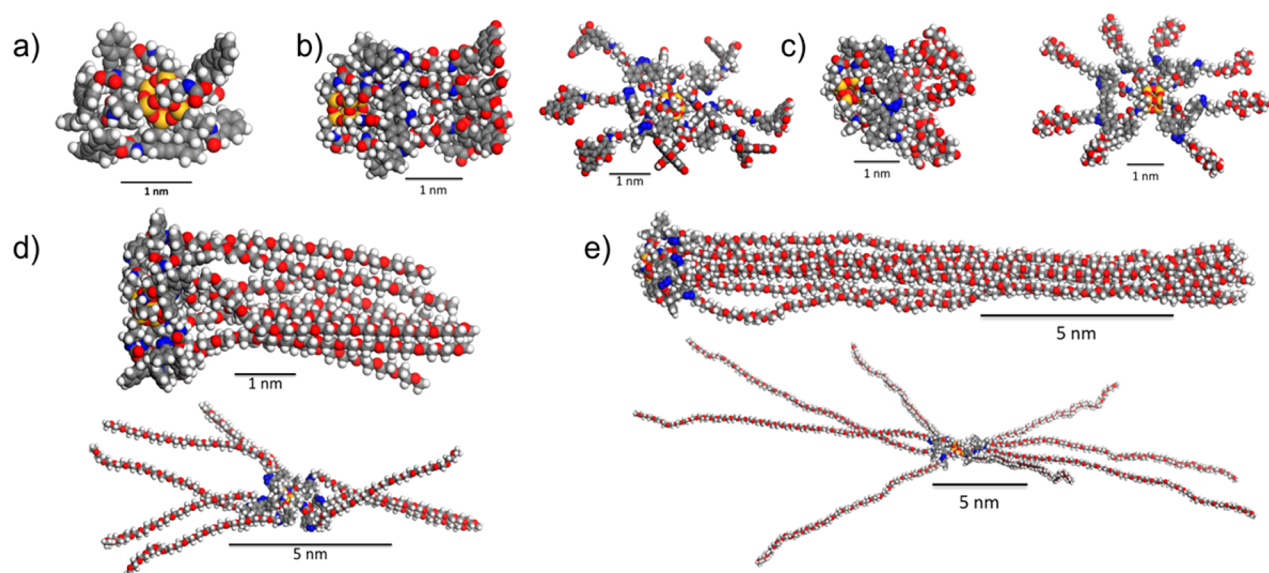


**Figure 3.** Molecular models of compounds: (a) 3; (b) 8: left-submerged, right-extended; (c) 9: left-submerged, right-extended; (d) 10: top-submerged, bottom-extended; (e) 11: top-submerged, bottom-extended.

**Table 2.** Experimentally Observed and Calculated Molecular Areas of Compounds 8–11 and Properties of LB Monolayers

compd	mol area, nm <sup>2</sup>			contact angle, deg		monolayer thickness, <sup>a</sup> nm	
	LB ( <i>A</i> <sub>0</sub> )	min cross section	max cross section	1 mN/m	4 mN/m	1 mN/m	4 mN/m
3		4.3					
8	10.2	5.0	30.4	91 ± 2	88 ± 1	1.15 ± 0.01	1.58 ± 0.03
9	4.9	4.7	25.4	33 ± 5	36 ± 6	1.29 ± 0.05	1.55 ± 0.03
10	33.4	5.3	138.8	49 ± 2	48.3 ± 0.7	0.91 ± 0.01	1.81 ± 0.04
11	87.6	6.0	789.6	45 ± 2	41 ± 1	0.91 ± 0.01	1.13 ± 0.04

<sup>a</sup>From spectroscopic ellipsometry.

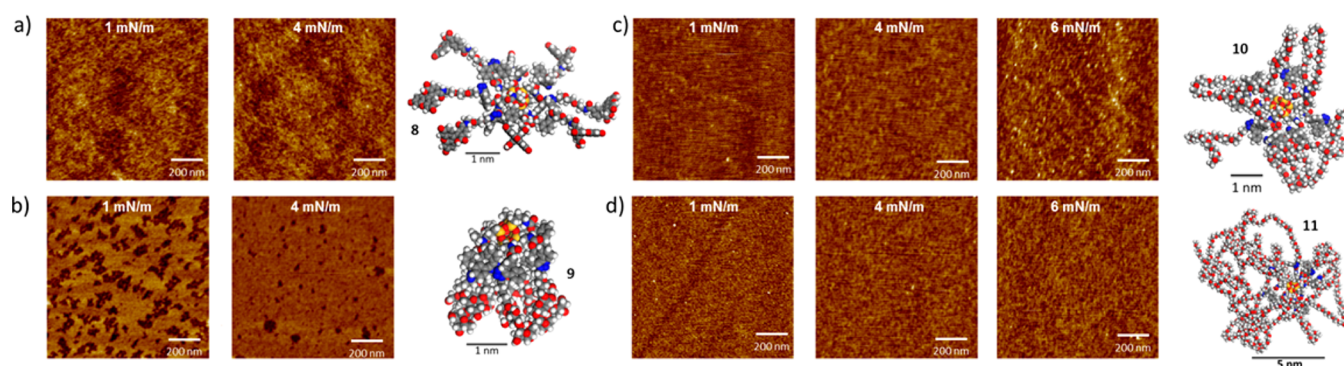


**Figure 4.**  $1 \times 1 \mu\text{m}^2$  AFM topographical images of LB monolayers deposited at 1, 4, and 6 mN/m for 8 (a), 9 (b), 10 (c), and 11 (d), and corresponding molecular models on the right. AFM Z-scale is 4 nm for 8 and 9 and 2 nm for 10 and 11.

and Table 2). As was found from the LB experiment, compounds 8 and 9 formed molecular monolayers with limiting cross-sectional area of 10.2 and 4.9 nm<sup>2</sup>, respectively, at higher surface pressure. The comparison of experimental data with modeling results indicates that the arms are submerged into the subphase at high compression, more so for compound 9 (minimum area = 4.7 nm<sup>2</sup>, observed 4.9 nm<sup>2</sup>) with hydrophilic lactose arms than for 8 (minimum area = 5.0 nm<sup>2</sup>, observed 10.2 nm<sup>2</sup>) bearing relatively hydrophobic fluorescein moieties. It can be therefore concluded that the POSS–fluorescein conjugate has a pancake-like conformation at the air–water interface (Figure 3b on the right), whereas compound POSS–lactose conjugate 9 behaves more like a

surfactant with polar end bearing lactose arms submerged into the subphase (Figure 3c on the left).

The amphipolar nature of poly(ethylene glycol) and relatively small weight fraction of hydrophobic segment resulted in gradual compression at lower pressures before the collapse of the monolayers of compounds 10 and 11, with corresponding limiting surface molecular areas of 33.4 and 87.6 nm<sup>2</sup>, respectively (Figure 2 and Table 2).<sup>56</sup> The hydrophobic weight fraction is 0.30 and 0.15 for 10 and 11, respectively. As may be expected from the molecular weight of the PEG arms, the long plateau is observed for the compound with the highest molecular weight (2000 g/mol) of PEG arms. Furthermore, the limiting surface areas are roughly proportional to the molecular



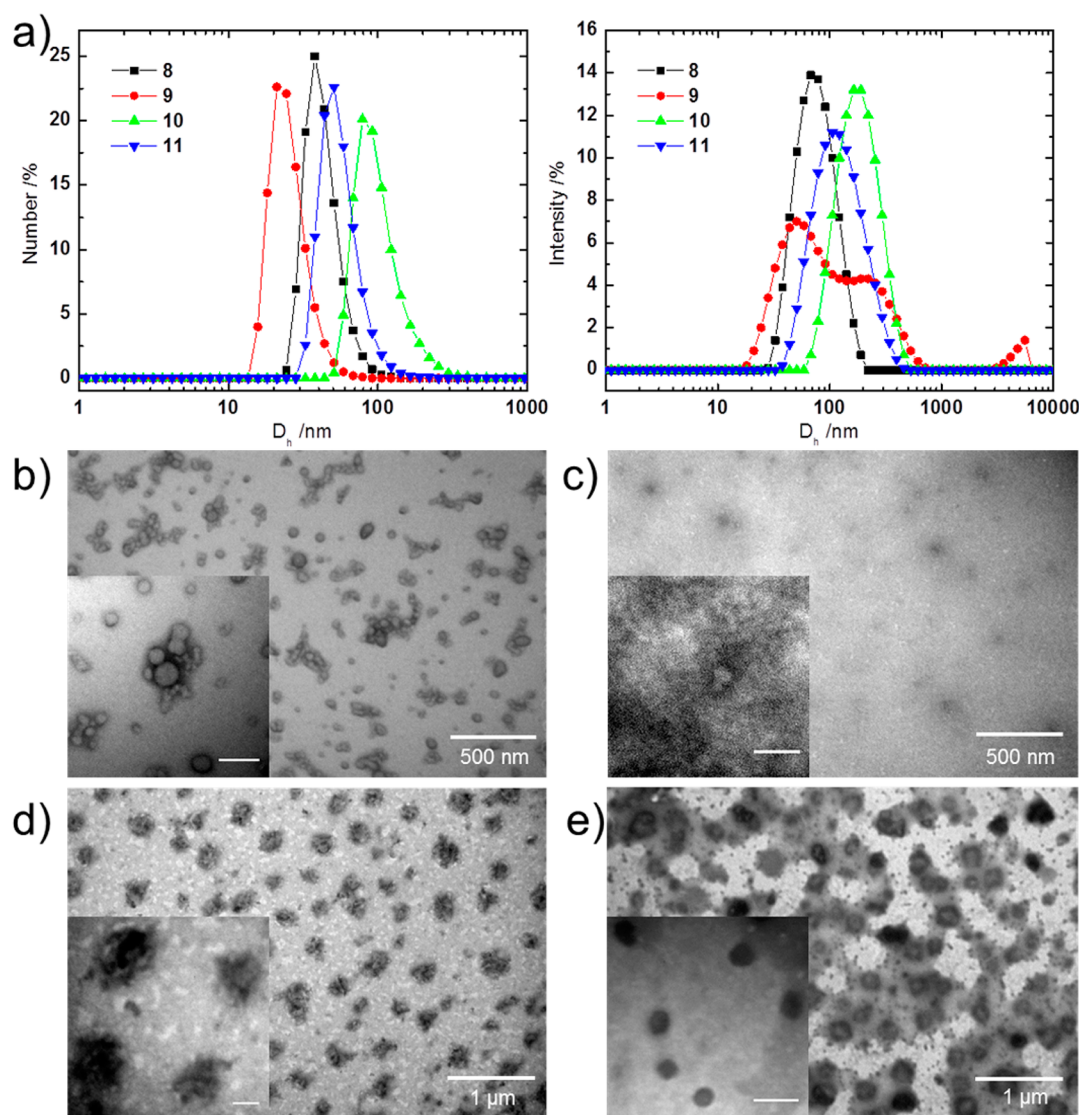


**Figure 5.** (a) Number-based (left) and intensity-based (right) size distributions of self-assemblies from compounds **8–11** in aqueous solution obtained with DLS method. (b) TEM image of self-assemblies from compound **8**. (c) TEM image of self-assemblies from compound **9**. (d) TEM image of self-assemblies from compound **10**. (e) TEM image of self-assemblies from compound **11**. The inset scale bars are 100 nm. Stained by phosphotungstic acid.

weight of POSS conjugates **10** and **11** and are similar if expressed in the surface area of the ethylene oxide repeat unit of about  $0.25 \text{ nm}^2$ . Considering the molecular areas obtained from modeling of compounds **10** ( $5.3\text{--}138.8 \text{ nm}^2$ ) and **11** ( $6.0\text{--}789.6 \text{ nm}^2$ ) and that the  $A_0$  obtained from LB are significantly larger than that of the POSS core, it is likely that the PEG chains are located predominantly at the interface in pancake-like conformation. Considering that low molecular weight poly(ethylene glycol)s ( $<90 \text{ kg/mol}$ ) normally do not form stable Langmuir monolayers, it is remarkable that POSS–PEG conjugates **10** and **11** are stable at the interface.<sup>57</sup> This stability could be in part due to the starlike architecture of the conjugates described here.<sup>58</sup>

The Langmuir monolayers were transferred onto silicon substrates at surface pressures of 1 and 4 mN/m and characterized with AFM (Figure 4a–e; also see Figure S4). As clear from these images, the fluorescein-modified POSS compound **8** formed a continuous LB monolayer with little molecular aggregation at 1 and 4 mN/m (Figures 4a and Figure S4a). The RMS microroughness of the ultrathin films ( $R_q$ ) over

$1 \mu\text{m}^2$  area was very low, around 0.4 nm, which is characteristic of molecularly uniform monolayers. The monolayer surface is hydrophobic with an advancing contact angle of  $91 \pm 2^\circ$  at 1 mN/m and  $88 \pm 1^\circ$  at 4 mN/m, thus indicating that the hydrophilic fluorescein–triethylene glycol arms interact with silicon substrate and hydrophobic POSS–DIBO fragments are exposed on the surface of the film (Table 2).

For compound **9**, the microroughness reduced from 0.48 nm at surface pressures of 1 mN/m to 0.21 nm at 4 mN/m, which indicates the transition to a solid phase with occasional pinhole defects and modestly hydrophilic character of mixed lactose and POSS cores (contact angle is around  $35^\circ$ ) (Figure 4b and Table 2). The LB monolayers of PEG–POSS compounds **10** and **11** showed an extremely smooth morphology with PEG chains forming a bicontinuous network on the air–water interface without pronounced segregation. The  $R_q$  of 0.17 nm for POSS–PEG films did not change even at surface pressure of 6 mN/m (Figure 4c,d). The hydrophilicity of POSS–PEG monolayers was similar to contact angle slightly lower for **11** with higher content of PEG arms ( $41 \pm 1^\circ$  vs  $48 \pm 0.7^\circ$  at 4

mN/m) (Table 2). The monolayer thickness increased with surface pressure from 1.1 to 1.6 nm for **8**, 1.3 to 1.5 nm for **9**, 0.9 to 1.8 nm for **10**, and 0.9 to 1.13 nm for **11** as determined by spectroscopic ellipsometry measurements (Table 2). Overall, all branched POSS compounds synthesized here show interfacial behavior, which is characteristic for branched amphiphiles.<sup>14</sup> The generalized conformations of compounds **8–11** on the air–water interface are presented in Figure 4a–c. The hydrophobic fluorescein arms of **8** are extended at the interphase, whereas the extremely hydrophilic lactose arms of **9** are submerged into subphase, resulting in the smallest  $A_0$  value of 4.9 nm<sup>2</sup>. The molecular monolayers from POSS–PEG derivatives **10** and **11** have PEG side chains at the interface at modest pressures but due to the smaller hydrophobic weight fraction are squeezed into a subphase at higher surface pressures.

**Assembly in Aqueous Solutions.** Next, we investigated the behavior of starlike POSS conjugates **8–11** in aqueous solutions. Compounds **8** and **9** were assembled by dissolving in DMSO followed by dialysis against water (3 kDa MWCO) with final concentration of ca. 1 mg/mL. The presence of self-assemblies was then evaluated using dynamic light scattering (DLS) and transmission electron microscopy (TEM) (Figure 5). Both compounds formed polydisperse nanostructures with a z-average hydrodynamic diameter ( $D_h$ ) of 69–76 nm (from DLS) (Table 1). The number-average diameter was found to be 43 nm for **8** and 26 nm for **9** which correlates well with the TEM data (Figure 5b,c). The compound **8** with fluorescein arms formed more uniform, predominantly vesicular structures with sizes of self-assemblies on the order of 50 nm, according to TEM. On the other hand, POSS **9** with hydrophilic lactose arms formed smaller micellar self-assemblies with sizes approximately 20 nm (Figure 5c). Furthermore, the intensity distribution of sizes of assemblies from compound **9** has a bimodal character that is reflected in high polydispersity index. It has to be noted that the examples of aqueous self-assembly of POSS conjugates with short organic arms are very rare, and the fact that compounds **8** and **9** yield stable nanostructures is rather remarkable.

Furthermore, POSS–PEG compounds **10** and **11** were added in a nonselective solvent (THF) to an excess of water and after evaporation of the organic solvent (final concentration 1 mg/mL), formed self-assemblies with a z-average diameter of 162 and 107 nm, respectively (Figure 5a and Table 1). The number-average diameter was found to be 103 and 57 nm for self-assemblies of **10** and **11**, respectively. The DLS data analysis thus shows that the molecule **10** having a smaller hydrophilic segment forms larger particles, whereas compound **11** yields self-assemblies of a smaller size. The longer hydrophilic PEG arms make compound **11** more stable in aqueous solution with a weaker tendency to aggregate and self-assemble.<sup>59</sup> Both POSS–PEG conjugates show collapsed structures in TEM images with sizes about 100 nm. Notably, the collapsed micellar structures formed from **10** are visible in Figure 5d, whereas the self-assemblies from compound **11** show vesicular morphology.

By using the light scattering data for solutions with different concentrations, we found that the critical micellar concentration for compounds **8** and **9** is approximately 2  $\mu$ M, which is significantly lower than that common for comparable linear compounds (Figure S5). POSS–PEG compounds **10** and **11** form assemblies at much higher concentrations, above 8 and 50  $\mu$ M, respectively, due to the presence of weakly interacting

PEG terminal blocks. Overall, compounds **9**, **10**, and **11** with large hydrophilic segments (lactose, 750 g/mol and 2000 g/mol PEG) showed rather poor stability and high polydispersity of aqueous assemblies due to the high hydrophilic to hydrophobic ratios. The partial functionalization of eight available alkyne groups of compound **3** with hydrophilic and hydrophobic moieties to give heterofunctionalized branched structures could lead to a more robust aqueous assembly that will be further investigated.

## CONCLUSIONS

In conclusion, we have synthesized the novel organic–inorganic monodisperse POSS scaffold **3** modified by eight pendant cyclooctyne groups that could be easily functionalized via a click-based approach with various azido compounds. We demonstrated that this approach can be applied to azide-containing fluorescent dye and hydrophilic moieties such as carboxyfluorescein, lactose, and PEGs to give a library of nearly monodisperse branched organic–inorganic hybrid nanoparticles a few nanometers in diameter. The conjugation of hydrophilic moieties to the POSS-based scaffold **3** resulted in diverse self-assembly behavior driven by the hydrophobic POSS core with the morphology of the structures dependent on the molecular weight and the type of the peripheral hydrophilic moieties. We suggest that rapid SPAAC coupling in the absence of a catalyst will facilitate the preparation of functional organic–inorganic nanoparticles suitable for many demanding applications where metal ion contamination is undesirable. For instance, clickable nanoparticles with high functional density and well-defined cubic cage structures are attractive as molecular building blocks and cross-linkers that can be employed without transition metal catalysis and do not produce toxic byproducts. Furthermore, the strain-promoted cycloadditions with other 1,3-dipoles such as nitrones and nitrile oxides can complement the functionalization strategy reported herein.

## ASSOCIATED CONTENT

### Supporting Information

Characterization information for compounds **4–7**; Figures S1–S5; mass spectra and NMR spectra. The Supporting Information is available free of charge on the ACS Publications website at DOI: 10.1021/acs.langmuir.5b01764.

## AUTHOR INFORMATION

### Corresponding Author

\*E-mail: vladimir@mse.gatech.edu (V.V.T.).

### Notes

The authors declare no competing financial interest.

## ACKNOWLEDGMENTS

This work was supported by National Science Foundation (NSF-DMR 1002810 to V.V.T.) and the National Cancer Institute of the US National Institutes of Health (R01CA88986 to G.-J.B.). We thank Dr. Nagesh Kolishetti and Manish Hudlikar for assistance with synthesis of the azides. We thank Chaowei Feng and Prof. Zhiqun Lin for assistance with GPC measurements.

## REFERENCES

- (1) Wu, J.; Mather, P. T. POSS Polymers: Physical Properties and Biomaterials Applications. *Polym. Rev.* **2009**, *49*, 25–63.



- (2) Wang, F. K.; Lu, X. H.; He, C. B. Some recent developments of polyhedral oligomeric silsesquioxane (POSS)-based polymeric materials. *J. Mater. Chem.* **2011**, *21*, 2775–2782.
- (3) Pielichowski, K.; Njuguna, J.; Janowski, B.; Pielichowski, J. Polyhedral Oligomeric Silsesquioxanes (POSS)-Containing Nano-hybrid Polymers. In *Advances in Polymer Science*; Springer: Berlin, 2006; Vol. 201, pp 225–296.
- (4) Cassagneau, T.; Caruso, F. Oligosilsesquioxanes as versatile building blocks for the preparation of self-assembled thin films. *J. Am. Chem. Soc.* **2002**, *124*, 8172–8180.
- (5) He, C.; Xiao, Y.; Huang, J.; Lin, T.; Mya, K. Y.; Zhang, X. Highly efficient luminescent organic clusters with quantum dot-like properties. *J. Am. Chem. Soc.* **2004**, *126*, 7792–7793.
- (6) Lo, M. Y.; Zhen, C.; Lauters, M.; Jabbour, G. E.; Sellinger, A. Organic-inorganic hybrids based on pyrene functionalized octavinyl-silsesquioxane cores for application in OLEDs. *J. Am. Chem. Soc.* **2007**, *129*, 5808–5809.
- (7) Pu, K. Y.; Li, K.; Liu, B. Cationic oligofluorene-substituted polyhedral oligomeric silsesquioxane as light-harvesting unimolecular nanoparticle for fluorescence amplification in cellular imaging. *Adv. Mater.* **2010**, *22*, 643–646.
- (8) Liras, M.; Pintado-Sierra, M.; Amat-Guerri, F.; Sastre, R. New BODIPY chromophores bound to polyhedral oligomeric silsesquioxanes (POSS) with improved thermo- and photostability. *J. Mater. Chem.* **2011**, *21*, 12803–12811.
- (9) Zhang, H. J.; Kulkarni, S.; Wunder, S. L. Polyethylene glycol functionalized polyoctahedral silsesquioxanes as electrolytes for lithium batteries. *J. Electrochem. Soc.* **2006**, *153*, A239–A248.
- (10) Tanaka, K.; Ishiguro, F.; Chujo, Y. POSS Ionic Liquid. *J. Am. Chem. Soc.* **2010**, *132*, 17649–17651.
- (11) Chinnam, P. R.; Wunder, S. L. Polyoctahedral Silsesquioxane-Nanoparticle Electrolytes for Lithium Batteries: POSS-Lithium Salts and POSS-PEGs. *Chem. Mater.* **2011**, *23*, 5111–5121.
- (12) Fabritz, S.; Horner, S.; Avrutina, O.; Kolmar, H. Bioconjugation on cube-octameric silsesquioxanes. *Org. Biomol. Chem.* **2013**, *11*, 2224–2236.
- (13) Zhang, W. A.; Muller, A. H. E. Architecture, self-assembly and properties of well-defined hybrid polymers based on polyhedral oligomeric silsesquioxane (POSS). *Prog. Polym. Sci.* **2013**, *38*, 1121–1162.
- (14) Peleshanko, S.; Tsukruk, V. V. The architectures and surface behavior of highly branched molecules. *Prog. Polym. Sci.* **2008**, *33*, 523–580.
- (15) Yu, X. F.; Li, Y. W.; Dong, X. H.; Yue, K.; Lin, Z. W.; Feng, X. Y.; Huang, M. J.; Zhang, W. B.; Cheng, S. Z. D. Giant Surfactants Based on Molecular Nanoparticles: Precise Synthesis and Solution Self-assembly. *J. Polym. Sci., Part B: Polym. Phys.* **2014**, *52*, 1309–1325.
- (16) Mya, K. Y.; Li, X.; Chen, L.; Ni, X.; Li, J.; He, C. Core-corona structure of cubic silsesquioxane-poly(ethylene oxide) in aqueous solution: fluorescence, light scattering, and TEM studies. *J. Phys. Chem. B* **2005**, *109*, 9455–9462.
- (17) Zhang, W. A.; Wang, S. H.; Li, X. H.; Yuan, J. Y.; Wang, S. L. Organic/inorganic hybrid star-shaped block copolymers of poly(L-lactide) and poly(N-isopropylacrylamide) with a polyhedral oligomeric silsesquioxane core: Synthesis and self-assembly. *Eur. Polym. J.* **2012**, *48*, 720–729.
- (18) Shih, R. S.; Lu, C. H.; Kuo, S. W.; Chang, F. C. Hydrogen Bond-Mediated Self-Assembly of Polyhedral Oligomeric Silsesquioxane-Based Supramolecules. *J. Phys. Chem. C* **2010**, *114*, 12855–12862.
- (19) Bothe, M.; Mya, K. Y.; Lin, E. M. J.; Yeo, C. C.; Lu, X. H.; He, C. B.; Pretsch, T. Triple-shape properties of star-shaped POSS-polycaprolactone polyurethane networks. *Soft Matter* **2012**, *8*, 965–972.
- (20) Zhang, C.; Guang, S.; Zhu, X.; Xu, H.; Liu, X.; Jiang, M. Mechanism of Dielectric Constant Variation of POSS-Based Organic-Inorganic Molecular Hybrids. *J. Phys. Chem. C* **2010**, *114*, 22455–22461.
- (21) Kim, D. G.; Kang, H.; Han, S.; Lee, J. C. The increase of antifouling properties of ultrafiltration membrane coated by star-shaped polymers. *J. Mater. Chem.* **2012**, *22*, 8654–8661.
- (22) Ledin, P. A.; Tkachenko, I. M.; Xu, W.; Choi, I.; Shevchenko, V. V.; Tsukruk, V. V. Star-shaped molecules with polyhedral oligomeric silsesquioxane core and azobenzene dye arms. *Langmuir* **2014**, *30*, 8856–8865.
- (23) Marciniak, B. Hydrosilylation: A Comprehensive Review on Recent Advances. *Adv. Silicon. Sci.* **2009**, *1*, 1–408.
- (24) Cordes, D. B.; Lickiss, P. D.; Rataboul, F. Recent developments in the chemistry of cubic polyhedral oligosilsesquioxanes. *Chem. Rev.* **2010**, *110*, 2081–2173.
- (25) Li, Y.; Zhang, W. B.; Hsieh, I. F.; Zhang, G.; Cao, Y.; Li, X.; Wesdemiotis, C.; Lotz, B.; Xiong, H.; Cheng, S. Z. Breaking symmetry toward nonspherical Janus particles based on polyhedral oligomeric silsesquioxanes: molecular design, “click” synthesis, and hierarchical structure. *J. Am. Chem. Soc.* **2011**, *133*, 10712–10715.
- (26) Fabritz, S.; Heyl, D.; Bagutski, V.; Empting, M.; Rikowski, E.; Frauendorf, H.; Balog, I.; Fessner, W. D.; Schneider, J. J.; Avrutina, O.; Kolmar, H. Towards click bioconjugations on cube-octameric silsesquioxane scaffolds. *Org. Biomol. Chem.* **2010**, *8*, 2212–2218.
- (27) Perez-Ojeda, M. E.; Trastoy, B.; Lopez-Arbeloa, I.; Banuelos, J.; Costela, A.; Garcia-Moreno, I.; Chiara, J. L. Click assembly of dye-functionalized octasilsesquioxanes for highly efficient and photostable photonic systems. *Chem. - Eur. J.* **2011**, *17*, 13258–13268.
- (28) Lo Conte, M.; Staderini, S.; Chambery, A.; Berthet, N.; Dumy, P.; Renaudet, O.; Marra, A.; Dondoni, A. Glycoside and peptide clustering around the octasilsesquioxane scaffold via photoinduced free-radical thiol-ene coupling. The observation of a striking glycoside cluster effect. *Org. Biomol. Chem.* **2012**, *10*, 3269–3277.
- (29) Trastoy, B.; Bonsor, D. A.; Perez-Ojeda, M. E.; Jimeno, M. L.; Mendez-Ardoy, A.; Fernandez, J. M. G.; Sundberg, E. J.; Chiara, J. L. Synthesis and Biophysical Study of Disassembling Nanohybrid Bioconjugates with a Cubic Octasilsesquioxane Core. *Adv. Funct. Mater.* **2012**, *22*, 3191–3201.
- (30) Perez-Ojeda, M. E.; Trastoy, B.; Rol, A.; Chiara, M. D.; Garcia-Moreno, I.; Chiara, J. L. Controlled click-assembly of well-defined hetero-bifunctional cubic silsesquioxanes and their application in targeted bioimaging. *Chem. - Eur. J.* **2013**, *19*, 6630–6640.
- (31) Debets, M. F.; van Berkel, S. S.; Dommerholt, J.; Dirks, A. T.; Rutjes, F. P.; van Delft, F. L. Bioconjugation with strained alkenes and alkynes. *Acc. Chem. Res.* **2011**, *44*, 805–815.
- (32) Sletten, E. M.; Bertozzi, C. R. From mechanism to mouse: a tale of two bioorthogonal reactions. *Acc. Chem. Res.* **2011**, *44*, 666–676.
- (33) Sanders, B. C.; Friscourt, F.; Ledin, P. A.; Mbua, N. E.; Arumugam, S.; Guo, J.; Boltje, T. J.; Popik, V. V.; Boons, G.-J. Metal-free sequential [3+ 2]-dipolar cycloadditions using cyclooctynes and 1,3-dipoles of different reactivity. *J. Am. Chem. Soc.* **2011**, *133*, 949–957.
- (34) Chen, W.; Wang, D.; Dai, C.; Hamelberg, D.; Wang, B. Clicking 1,2,4,5-tetrazine and cyclooctynes with tunable reaction rates. *Chem. Commun.* **2012**, *48*, 1736–1738.
- (35) Heaney, F. Nitrile Oxide/Alkyne Cycloadditions - A Credible Platform for Synthesis of Bioinspired Molecules by Metal-Free Molecular Clicking. *Eur. J. Org. Chem.* **2012**, *2012*, 3043–3058.
- (36) MacKenzie, D. A.; Sherratt, A. R.; Chigrinova, M.; Cheung, L. L.; Pezacki, J. P. Strain-promoted cycloadditions involving nitrones and alkynes—rapid tunable reactions for bioorthogonal labeling. *Curr. Opin. Chem. Biol.* **2014**, *21*, 81–88.
- (37) Such, G. K.; Johnston, A. P. R.; Liang, K.; Caruso, F. Synthesis and functionalization of nanoengineered materials using click chemistry. *Prog. Polym. Sci.* **2012**, *37*, 985–1003.
- (38) Lallana, E.; Fernandez-Trillo, F.; Sousa-Herves, A.; Riguera, R.; Fernandez-Megia, E. Click chemistry with polymers, dendrimers, and hydrogels for drug delivery. *Pharm. Res.* **2012**, *29*, 902–921.
- (39) Ledin, P. A.; Kolishetti, N.; Boons, G. J. Multi-Functionalization of Polymers by Strain-Promoted Cycloadditions. *Macromolecules* **2013**, *46*, 7759–7768.

- (40) Ledin, P. A.; Kolishetti, N.; Hudlikar, M. S.; Boons, G. J. Exploring strain-promoted 1,3-dipolar cycloadditions of end functionalized polymers. *Chem. - Eur. J.* **2014**, *20*, 8753–8760.
- (41) Li, Y. W.; Wang, Z.; Zheng, J. K.; Su, H.; Lin, F.; Guo, K.; Feng, X. Y.; Wesdemiotis, C.; Becker, M. L.; Cheng, S. Z. D.; Zhang, W. B. Cascading One-Pot Synthesis of Single-Tailed and Asymmetric Multitailed Giant Surfactants. *ACS Macro Lett.* **2013**, *2*, 1026–1032.
- (42) Su, H.; Zheng, J.; Wang, Z.; Lin, F.; Feng, X.; Dong, X.-H.; Becker, M. L.; Cheng, S. Z. D.; Zhang, W.-B.; Li, Y. Sequential Triple “Click” Approach toward Polyhedral Oligomeric Silsesquioxane-Based Multiheaded and Multitailed Giant Surfactants. *ACS Macro Lett.* **2013**, *2*, 645–650.
- (43) Su, H.; Li, Y. W.; Yue, K.; Wang, Z.; Lu, P. T.; Feng, X. Y.; Dong, X. H.; Zhang, S.; Cheng, S. Z. D.; Zhang, W. B. Macromolecular structure evolution toward giant molecules of complex structure: tandem synthesis of asymmetric giant gemini surfactants. *Polym. Chem.* **2014**, *5*, 3697–3706.
- (44) Li, Y. W.; Su, H.; Feng, X. Y.; Yue, K.; Wang, Z.; Lin, Z. W.; Zhu, X. L.; Fu, Q.; Zhang, Z. B.; Cheng, S. Z. D.; Zhang, W. B. Precision synthesis of macrocyclic giant surfactants tethered with two different polyhedral oligomeric silsesquioxanes at distinct ring locations via four consecutive “click” reactions. *Polym. Chem.* **2015**, *6*, 827–837.
- (45) Ledin, P. A.; Friscourt, F.; Guo, J.; Boons, G. J. Convergent assembly and surface modification of multifunctional dendrimers by three consecutive click reactions. *Chem. - Eur. J.* **2011**, *17*, 839–846.
- (46) Sheller, N. B.; Petrash, S.; Foster, M. D.; Tsukruk, V. V. Atomic force microscopy and X-ray reflectivity studies of albumin adsorbed onto self-assembled monolayers of hexadecyltrichlorosilane. *Langmuir* **1998**, *14*, 4535–4544.
- (47) McConney, M. E.; Singamaneni, S.; Tsukruk, V. V. Probing Soft Matter with the Atomic Force Microscopies: Imaging and Force Spectroscopy. *Polym. Rev.* **2010**, *50*, 235–286.
- (48) Feher, F. J.; Wyndham, K. D.; Soulivong, D.; Nguyen, F. Syntheses of highly functionalized cube-octameric polyhedral oligosilsesquioxanes (R<sub>8</sub>Si<sub>8</sub>O<sub>12</sub>). *J. Chem. Soc., Dalton Trans.* **1999**, 1491–1497.
- (49) Mbua, N. E.; Guo, J.; Wolfert, M. A.; Steet, R.; Boons, G. J. Strain-promoted alkyne-azide cycloadditions (SPAAC) reveal new features of glycoconjugate biosynthesis. *ChemBioChem* **2011**, *12*, 1912–1921.
- (50) Ning, X.; Guo, J.; Wolfert, M. A.; Boons, G. J. Visualizing metabolically labeled glycoconjugates of living cells by copper-free and fast Huisgen cycloadditions. *Angew. Chem., Int. Ed.* **2008**, *47*, 2253–2255.
- (51) Takahashi, M.; Odagi, T.; Tomita, H.; Oshikawa, T.; Yamashita, M. Synthesis and photoluminescence study of anthracene based dendrimer and dendron. *Tetrahedron Lett.* **2003**, *44*, 2455–2458.
- (52) Lakowicz, J. R.; Malicka, J.; D’Auria, S.; Gryczynski, I. Release of the self-quenching of fluorescence near silver metallic surfaces. *Anal. Biochem.* **2003**, *320*, 13–20.
- (53) Se, K.; Takuya, S.; Ogawa, E. Molecular weight determination of star polymers and star block copolymers using GPC equipped with low-angle laser light-scattering. *Polymer* **2002**, *43*, 5447–5453.
- (54) Gunawidjaja, R.; Huang, F.; Gumenna, M.; Klimenko, N.; Nunnery, G. A.; Shevchenko, V.; Tannenbaum, R.; Tsukruk, V. V. Bulk and surface assembly of branched amphiphilic polyhedral oligomer silsesquioxane compounds. *Langmuir* **2009**, *25*, 1196–1209.
- (55) Anderson, P. M.; Wilson, M. R. Molecular dynamics simulations of amphiphilic graft copolymer molecules at a water/air interface. *J. Chem. Phys.* **2004**, *121*, 8503–8510.
- (56) Joncheray, T. J.; Denoncourt, K. M.; Mathieu, C.; Meier, M. A.; Schubert, U. S.; Duran, R. S. Langmuir and Langmuir-Blodgett films of poly(ethylene oxide)-b-poly(epsilon-caprolactone) star-shaped block copolymers. *Langmuir* **2006**, *22*, 9264–9271.
- (57) Lee, W.; Ni, S.; Deng, J.; Kim, B.-S.; Satija, S. K.; Mather, P. T.; Esker, A. R. Telechelic Poly(ethylene glycol)-POSS Amphiphiles at the Air/Water Interface. *Macromolecules* **2007**, *40*, 682–688.
- (58) Gunawidjaja, R.; Peleshanko, S.; Genson, K. L.; Tsitsilianis, C.; Tsukruk, V. V. Surface morphologies of Langmuir-Blodgett monolayers of PEOnPSn multiarm star copolymers. *Langmuir* **2006**, *22*, 6168–6176.
- (59) Discher, D. E.; Eisenberg, A. Polymer vesicles. *Science* **2002**, *297*, 967–973.